Case Studies in Construction Materials 22 (2025) e04576

Contents lists available at ScienceDirect

Case Studies in Construction Materials

journal homepage: www.elsevier.com/locate/cscm

Design and construction of high-performance surface textures for precast concrete pavements: A flexible formwork and 3D printing assisted texturing method

Xingyu Chen [a,1], Yuhong Wang [a,2,*], Xingyi Zhu [b], Wei Sheng [a], Long Yee Chan [a]

[a] Department of Civil and Environmental Engineering, The Hong Kong Polytechnic University, Hung Hom, Kowloon, Hong Kong
[b] The Key Laboratory of Road and Traffic Engineering of Ministry of Education, Tongji University, Shanghai 201804, China

ARTICLE INFO

Keywords:
Precast concrete pavements
Surface textures
3D printing technology
Noise reduction
Skid resistance

ABSTRACT

Surface textures are critical to the skid resistance and noise reduction of precast concrete pavements (PCPs). However, due to the constraints of current texturing technologies, only limited types of simple textures are produced for PCP. To facilitate the design and construction of superior textures for PCP, a novel texturing method assisted with 3D printing (3DP) technology is developed in this study. The process begins with using 3DP technology to construct the solid molds with customized textures. Subsequently, liquid silicone rubber is poured into solid molds to produce flexible formworks. The solidified flexible formworks are then employed to imprint textures onto the PCPs surfaces. To assess the impact of textures on the surface performance of PCPs, seven distinct texture designs were created and evaluated for their skid resistance and noise reduction performance. The findings reveal that texture configuration significantly influences PCPs' surface performance. Additionally, a full-scale trial section of PCPs was constructed to determine the practicality of this texturing technique, and the associated costs were analyzed as well. It is found that the textures created on the trial section of PCPs are of high quality, and the expenses incurred by this texturing method are competitive with those of traditional techniques. Therefore, this texturing method is promising to reform the design and construction of surface textures for PCPs.

1. Introduction

Precast concrete pavements (PCPs) have been increasingly constructed for highways, airports, and streets [1–4]. PCPs are manufactured in the factory and then transported and installed on-site. Quick construction and maintenance of PCPs minimizes the construction-related disruption and extends the service life of pavements. Along with the rising demands of modular and intelligent pavements, PCPs are supposed to be the principal type of pavements in the future. Numerous studies have been conducted to enhance the connection and structure performance of PCPs [5–9], however, the surface performance of PCPs is less researched, although it is critical to the traffic safety and driving comfort.

* Corresponding author.
E-mail addresses: xingyu666.chen@connect.polyu.hk (X. Chen), yuhong.wang@polyu.edu.hk (Y. Wang), zhuxingyi66@tongji.edu.cn (X. Zhu), ceewei.sheng@connect.polyu.hk (W. Sheng), ahdacly.chan@connect.polyu.hk (L.Y. Chan).
[1] ORCID: https://orcid.org/0000-0002-5828-7302.
[2] ORCID: https://orcid.org/0000-0002-4506-4230.

https://doi.org/10.1016/j.cscm.2025.e04576
Received 17 December 2024; Received in revised form 13 March 2025; Accepted 23 March 2025
Available online 24 March 2025

Typical surface functions of PCPs include skid resistance, noise reduction, and drainage. In the United States, more than 5,891,000 vehicle crashes happened each year from 2007 to 2016, 15 % of which were related to skid resistance loss [10]. As for the tire-pavement noise, it occupies nearly 41 % of the noise generated by a car [11]. Surface drainage is also critically important. If surface water cannot be drained timely, a water film may form on road surface during rainy conditions, leading to hazardous vehicle hydroplaning. Thus, more attention should be paid to improve the surface performance of PCPs. The surface performance of PCPs is highly dependent on the configuration of surface textures. Well-designed surface textures can effectively strengthen the skid resistance, mitigate the tire-pavement noise, and facilitate surface drainage of PCPs, but research or practices on finding high-performance surface textures are very limited. This is mainly due to the constraints of current texturing techniques.

The strategies of current texturing techniques for PCPs can be categorized into two types [12]: One is to scrape concrete in its plastic state, and the other is to carve concrete in its hardening state. The process of scraping concrete in its plastic state is to drag rough materials on the pavement surface manually or by using an automatic machine. These types of texturing techniques include burlap drag, transverse tining, longitudinal tining, and artificial turf drag [12–14]. Different to dragging rough materials on concrete in its plastic state, grinding and sawing machines are utilized in the second strategy to carve textures on the pavement surface when concrete is hardened. Diamond grinding and diamond grooving are two commonly used techniques for this purpose [15–18]. In diamond grinding, spaced blades rotated by a driving shaft are used to grind the concrete. The shape of ground textures is like a series of dosh lines at a resolution below 3 mm [19]. Similar to diamond grinding, in diamond grooving, straight blades are rotated to saw the concrete directly, but the pattern of the textures is in straight lines. Current construction methods and machines only allow the production of limited types of simple texture configurations. As a result, most of the texture optimization protocols are constrained in the adjustments of textures' dimensions, such as the width, mean profile depth, and space of the pavement textures [20–23]. Although the texture configuration plays an important role on the performance of pavement textures, the lack of advanced construction methods to freely create delicate textures limits the optimization of textures' configurations.

Flexible formwork technology can be referenced to create complicated surface textures on PCPs, since it has been widely employed in the concrete industry to construct structures with complex geometries. For instance, Cauberg et al. [24] used fabric flexible formworks to customize and control the shape of columns. Kromoser and Kollegger [25] created double-curvature domes from flat segments with the assistance of pneumatic formworks. Veenendaal and Block [26] innovated a flexible formwork system to produce the shell structure for large-span roofs and bridges. These flexible formwork technologies break the restrictions of structural and architectural shapes for concrete products. However, the customization of PCPs' surface textures requires high construction precision, which is hard to satisfy for these general flexible formworks. Thus, Hawkins et al. [27] pointed out that the flexible formwork technology should be combined with other advanced manufacturing technologies, such as 3D printing (3DP) technology, to enhance its construction and geometric flexibility.

3DP technology enables the customization of construction processes, which has created a revolution in manufacturing industries [28–30]. Compared to conventional texturing techniques for PCPs, 3DP technology provides distinctive advantages. For example, 3DP technology reduces labor requirements, eliminates the need for formwork, saves time, and provides flexibility in designing structures with intricate profiles [31–33]. However, the uptake of 3DP technology in PCPs is still limited. Contour crafting (CC) is one of the major 3DP techniques used in the concrete construction industries. The principle of CC is to extract cementitious paste to construct buildings layer by layer. The cementitious paste needs to have high workability for extrusion, yet its hardening process should be rapid enough to support the subsequent layers [30,34]. CC has the potential to be applied in the construction of PCPs, but it is not suitable to construct the surface textures of PCPs due to the high demands on printing resolution for textures. The six-axis robotic arm printer may be capable of fabricating complex textures on PCPs because it gives the designer more freedom to design the texture configurations on PCPs [35]. As the progressing of technology and the reduction of cost for the six-axis robotic arm printer, this device presents high potentials to modify the texture construction in PCPs. However, it is still not mature to directly manufacture surface textures on PCPs using the 3DP technology. A more technology-feasible and cost-effective approach is needed to facilitate the application of 3DP technology on the construction of PCPs' surface textures.

Motivated by the challenges mentioned above, the flexible formwork technology and 3DP technology were combined in this study to advance the surface texturing techniques of PCPs. Compared to the existing texturing methods, the proposed novel texturing method can give the designer more freedom to design the configuration of pavement textures and construct the designed textures on actual road. Not only the designed textures can be precisely manufactured, but certain delicate texture patterns can also be built, which are impossible by using the traditional texturing techniques. As a result, it is anticipated that the functionalities of pavement textures can be significantly improved. Specifically, 3D printing technology was employed to fabricate solid formworks with customized surface textures. These pre-textured solid formworks were then utilized to create textured flexible formworks. Finally, these textured flexible formworks were applied in the casting of PCPs. Seven distinct textures were designed and manufactured using this texturing method—mainly to evaluate the feasibility of the developed methodology and preliminary evaluate the impacts of textures on pavement's functional performance. The skid resistance and noise reduction performance of the textures were characterized to assess the impacts of texture configurations on the surface performance of PCPs. The surface drainage of the textures was not specifically tested, but a full-scale trial section of PCPs was constructed to evaluate the constructability of this texturing method, drainage, and the associated costs. The findings indicate that the textures produced on the test segment of PCPs are of superior quality, and the associated costs of this texturing approach are competitive with conventional methods. Conclusively, this texturing method has high potential to reform the design and construction of PCPs' surface textures.

2. Methodology

2.1. General working procedure

As aforementioned, the fundamental principle of using 3DP technology to create PCPs' textures involves making formworks that act as templates for the desired texture. Considering the convenience of demolding for textured formworks, the template materials must be flexible to allow easy removal from the hardened concrete. Directly manufacturing flexible formworks with 3DP technology is not feasible due to the limitation of computer-aided design (CAD) software in designing complex soft matters [36]. Therefore, a balanced strategy is proposed to address this dilemma. Firstly, a solid mold with customized texture configuration is designed using CAD software and constructed with the assistance of 3DP technology. Then, the pre-textured solid mold is served as a template for the preparation of flexible formworks. Specifically, a flexible material such as silicone rubber in its fluid state is grouted into the printed solid mold. Once the silica gel solidifies, it can be used as the surface formwork of PCPs' formwork system to cast the PCPs' slabs. After the concrete cures, the flexible formwork can be demolded and stored for future use. The manufactured PCPs' slabs will then be transported to the construction site for further assembly with the necessary joints. The joints are essential elements for the success of assembling textured PCP slabs, where a demountable stainless steel bar connection system has been well designed and introduced in another study [37]. Fig. 1 illustrates the general working procedure of this texturing method.

2.2. Prototype development at the laboratory scale

Following the general working procedure, this texturing method is applied in the laboratory to make textured samples for experimental tests. Seven types of textures were designed and constructed on the surface of concrete samples. Fig. 2 shows the appearances of the designed cylindrical samples and their corresponding cross-sectional details, including texture shape, dimension, and distances between textures. After the samples were fabricated, the British pendulum test and the noise absorption coefficient test were conducted to characterize the noise-reduction performance and skid-resistance performance of pavement, respectively. Cylindrical samples of 98 mm in diameter were used for the noise test, and rectangular samples of 168 mm in length and 98 mm in width were used for the skid resistance test. Cylindrical samples and rectangular samples shared the same texture configurations designed by a commonly used CAD software, CATIA.

The main reason of selecting these seven types of textures is to demonstrate that the proposed texturing method can help the designer more freely to design the configuration of pavement textures. Some of the textures are difficult or impossible to construct using traditional texturing techniques but may be effective for the performance modification of pavement textures. For example, the texture configuration of type 5 is a cavity with a narrow opening and a broadened body, which is difficult to construct using traditional texturing techniques. Compared to traditional texture configurations, this cavity-shaped structure may increase the reflection time of acoustic waves within textures [38,39]. As a result, the noise-reduction performance of pavement textures may be improved. Furthermore, to investigate the effects of textures' configurations on the skid-resistance and noise-reduction performance of pavement textures. The texture space of all designs are set at 14 mm, but the configuration of them are different. According to the texture configurations, these seven textures are divided into three groups. Type 1 and type 2 are classified into group 1, which uses holes as the major form of configurations. Type 3, type 4, and type 5 are classified into group 2, uses different grooves to form the textures. Type 6 and type 7 are classified into group 3, which combines grooves and holes as the textures. Additionally, specimens with flat surfaces are made to serve as the control sample for comparison purposes.

Once the texture configurations are identified, the 3D models of these textures are imported into a 3D printer for fabrication. In this study, a commercial 3D printer (Makerbot Replicator+) equipped with a smart extruder was used to fabricate the solid mold based on the fused deposition modeling (FDM) technology and shown in Fig. 3a. FDM was developed in the United States by Stratasys in the 1990s [40]. Compared with other 3DP techniques, the manufacturing process of FDM is more straightforward [41]. Firstly, thermoplastic polymers are heated into a semi-molten state for extrusion from a nozzle. Subsequently, the computer-controlled nozzle moves in the X, Y, and Z directions to construct the product layer-by-layer. Typically, acrylonitrile butadiene styrene (ABS) is used as the printing material in FDM, but this material tends to generate curling. Therefore, polylactic acid (PLA) filament with a diameter of 1.75 mm was chosen to substitute the ABS in this study. Considering that the melting temperature for PLA is 150–160 °C, the nozzle of

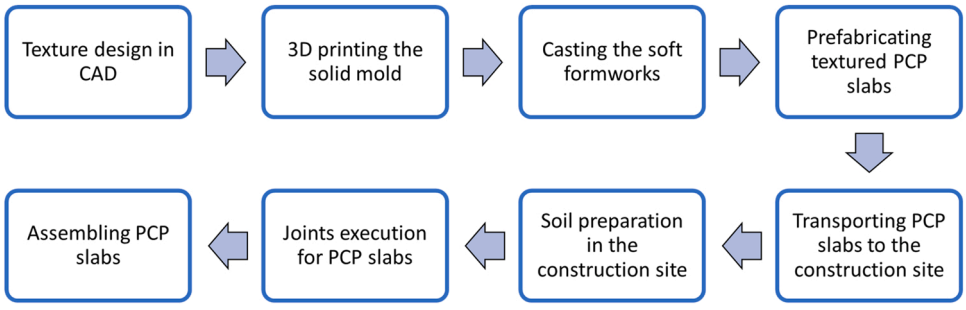

Fig. 1. General working procedure of the texturing method for PCPs.

	Type No.	Surface texture	Appearance	Cross-section
Group 1	1	Cylindrical holes		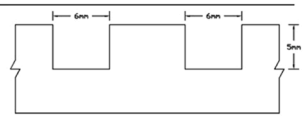
	2	Hemispherical holes	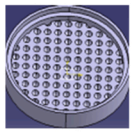	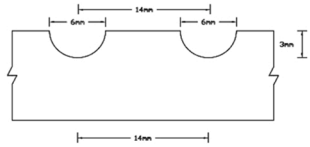
	3	Rectangular grooves	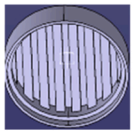	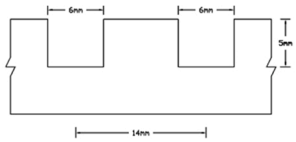
Group 2	4	Rectangular & hemispherical grooves	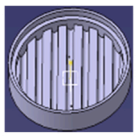	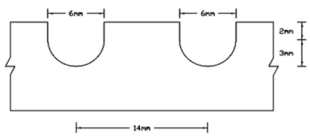
	5	Arc grooves	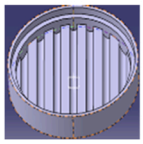	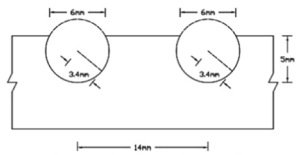
Group 3	6	Rectangular grooves with cylindrical holes	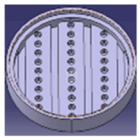	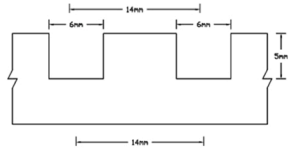
	7	Rectangular grooves with hemispherical holes		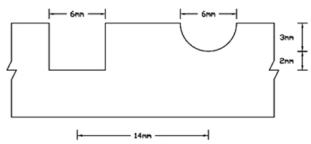

Fig. 2. Appearances and cross-sectional details of designed textures.

the smart extruder was heated to 210 °C to fuse PLA thoroughly. Guided by data from the 3D models, the smart extruder controls the extrusion rate and moving positions to construct the basic mold layer-by-layer. The finally produced cylindrical and rectangular molds are shown in Figs. 3b and 3c, respectively, and one of the detailed basic molds are shown in the right corner of Fig. 3a.

Fabricated solid molds were then utilized to create flexible formworks. The producing process of flexible formworks was presented in Fig. 4. BLUESIL™ RTV-3040, a commercial product of silicone rubber, was used as the material to create the flexible formworks. BLUESIL™ RTV-3040 is composed of two components: Part A is the base component, and part B is the catalyst component. The viscosities of these two components are so high (50,000 mPa.s for part A, 40,000 mPa.s for part B) that a motor stirrer is needed for mixing. Recommended by the customer handbook of BLUESIL™ RTV-3040 from the Freeman Manufacturing & Supply Company, the mix ratio by weight of part A and part B is set to be 10–1. At this proportion, BLUESIL™ RTV-3040 can have a one-hour time window at 24 °C for the base component and catalyst component to be thoroughly mixed.

During the mixing process, some air bubbles are trapped in the mixtures, which may create defects inside of the formworks and eventually affect its strength and durability. Hence, removing the trapped air is an essential step in creating flexible formworks. Firstly, a container with well-mixed mixtures was put into a chamber, and then a vacuum pump capable of achieving 73.6 cm of mercury vacuum was operated for deaeration. After deaeration, the mixtures were set in the vacuum chamber for another 2 minutes, and then they were poured out into the basic solid molds for curing. After curing for 24 hours at room temperature, the flexible formworks can be taken out for further use. Table 1 shows several typical properties of the cured rubber mixtures. Benefits from the superior mechanical performance and light weight of PCP slabs, the deform of flexible formworks under the weight of the cast concrete might be

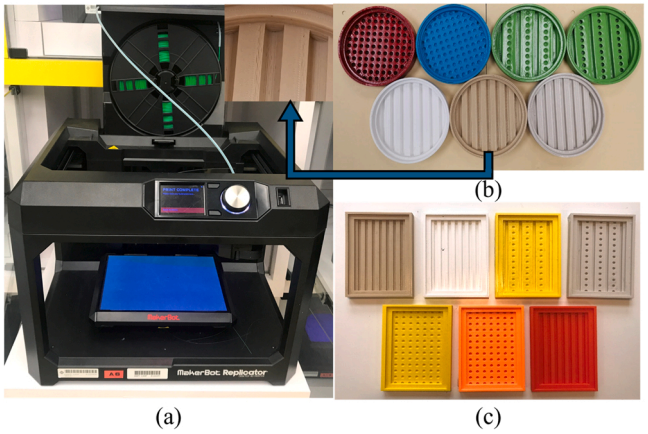

Fig. 3. Appearances of 3D-printed basic molds: (a) a commercial 3D printer (Makerbot Replicator+); (b) basic molds for making noise test specimens; (c) basic molds for making skidding test specimens.

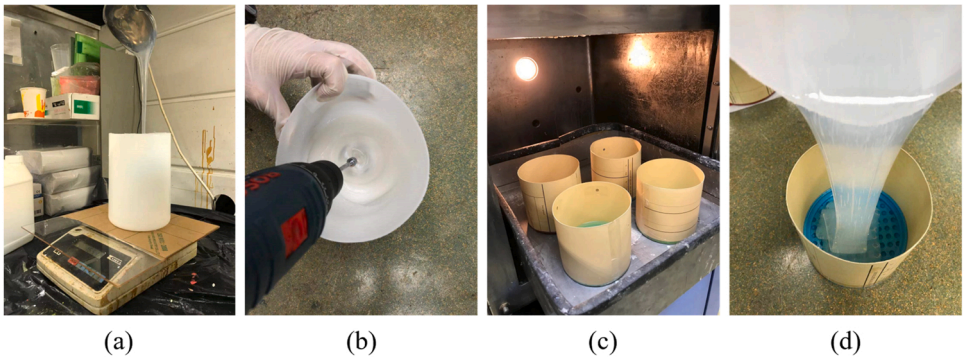

Fig. 4. The process of developing flexible formworks: (a) weighing part A and part B; (b) stirring the mixtures; (c) removing the trapped air; (d) pouring out the mixtures.

Table 1
Several typical properties of the cured rubber mixtures.

Property	Test Method	Value
Specific Gravity		1.08
Hardness	ASTM D2240	38
Tensile Strength, psi (N/mm^2)	ASTM D412	920 (6.3)
Elongation (%)	ASTM D412	340
Tear Resistance, ppi (N/mm)	ASTM D624, Die B	120 (21)
Linear Shrinkage, (%) (24 hours)		< 0.1
Linear Shrinkage, (%) (7 Days)		< 0.1
Temperature Range,°C		−54–204

neglected. Thus, to ensure the precision of flexible molds, the material used should achieve a critical balance: sufficient stiffness to resist deformation induced by concrete weight and construction activities and adequate flexibility to prevent surface damage during demolding. Moreover, based on the demolding experience, it is suggested to demold with a controlled peeling process (slowly tear inward along the four sides) to preserve the edge sharpness. The formed flexible formworks with customized configuration were shown in Fig. 5.

The flexible formworks created above were used to assemble the entire formworks for fresh concrete. Traditional materials such as wood, steel, or polyvinyl chloride (PVC) can still be used for the wall of the formworks. The flexible formworks were used as the lining of the entire formworks at the bottom. To save concrete curing time, sulfoaluminate cement (SAC), a high-performance cement (HPC), was used to make concrete specimens. The SAC used in this study is a commercial product from Tangshan Polar Bear Building Materials Co. Ltd, China, with a grade of 52.5, indicating a 28-day compressive strength of at least 52.5 MPa [42]. In addition to SAC, silica fume (SF), fly ash (FA), and superplasticizer (SP) were also part of the ingredients. Specifically, the mixing formula consists of 75 % SAC, 20 % FA, 5 % SF, and 1 % (by the weight of cementitious materials) SP, and the water-cement ratio is 0.3. After being cured, the

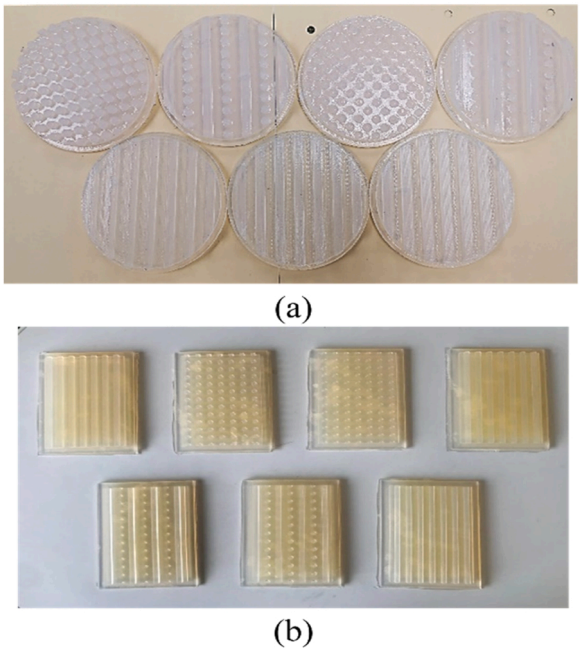

Fig. 5. The produced flexible formworks: (a) flexible cylindrical formworks; (b) flexible rectangular formworks.

hardened concrete samples were used for the noise absorption coefficient test and the British pendulum friction test. Benefits from the high early strength of this concrete material (54.8 MPa for 7-day compressive strength and 56.3 MPa for 28-day compressive strength), the created samples can be applied for the performance tests after only a week. More details about the sample preparation processes and the created samples are shown in Fig. 6.

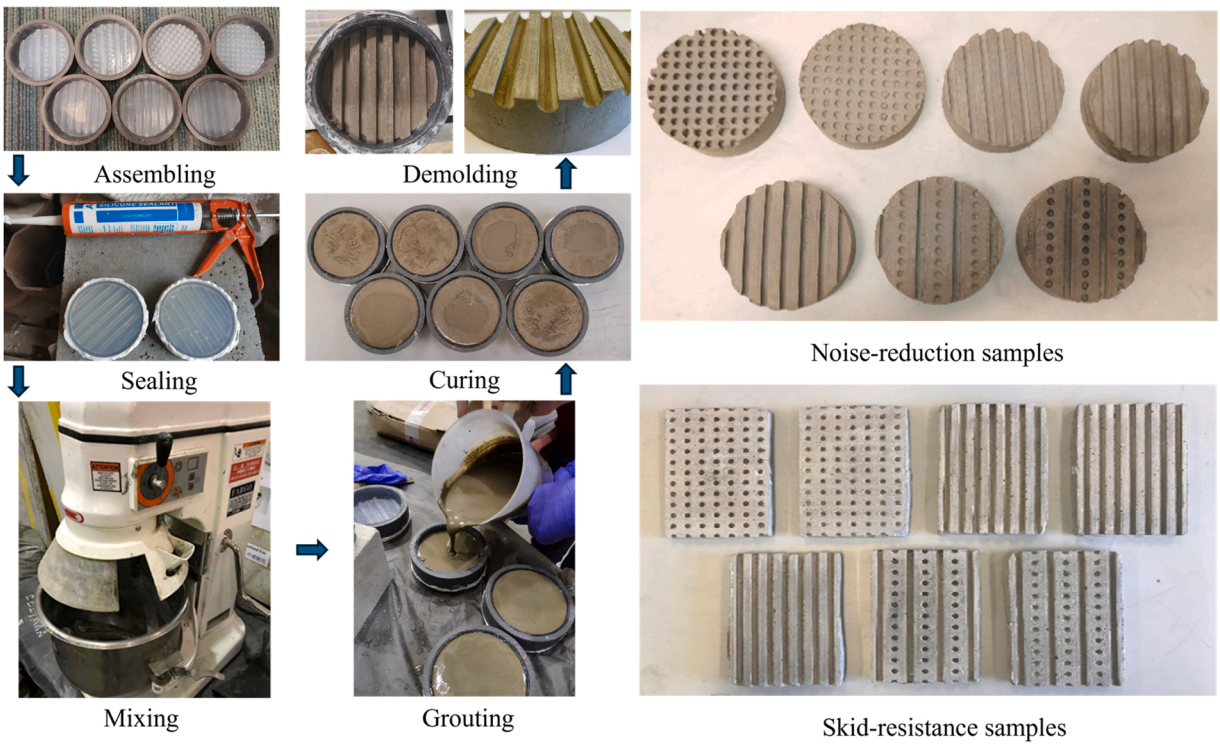

Fig. 6. The procedures for the sample preparation.

3. Experimental tests

3.1. Noise absorption coefficient test

A commercial impedance tube kit noted as type 4206 was used to test the noise absorption coefficient of specimens according to standard ASTM E1050, which is shown in Fig. 7. In performing the test, a loudspeaker was placed at one end of the tube to generate broadband sound waves, and a backplate was placed on the opposite end to mount the specimen. When sound waves hit the specimen, some were absorbed, and the others were reflected to interfere with the original forward-traveling waves. Thus, a new type of wave was formed in the tube. Meanwhile, a digital frequency analyzer was used to identify the function of the new wave. By analyzing the new type of waves, the noise absorption coefficient of the specimen can be identified. Specifically, sound pressure signals at the two locations obtained by microphones are transferred to a wave function, as shown in Eq. 1.

$$\overline{H} = \frac{G_{12}}{G_{11}} = |\overline{H}|e^{j\overline{\varphi}} \tag{1}$$

Where, $\overline{H}$ is the transfer function based on the two microphone signals, G_{11} is the auto power spectra of the acoustic pressure signal at the two microphone locations, G_{12} is the cross-power spectrum of the acoustic pressure signals at the two microphone locations, j is equal to $\sqrt{-1}$, $\overline{\varphi}$ is the measured phase of the complex transfer function.

Through a series of calculation steps guided by the ASTM E1050, the reflection coefficient under different frequencies of sound can be obtained. According to the relationship between the absorption coefficient and the reflection coefficient shown in Eq. 2, the absorption coefficient under different sound frequencies can be obtained to analyze the noise reduction performance of different pavement textures.

$$\alpha = 1 - R^2 \tag{2}$$

Where ɑ is the noise absorption coefficient, and R is the complex noise reflection coefficient.

Typically, the size of the backplate determines the range of testing frequencies. Considering that the frequency range of tire-pavement noise is from 500 Hz to 1500 Hz, a backplate with a diameter of 100 mm was chosen in this experiment, corresponding to testing frequencies from 50 Hz to 1600 Hz.

3.2. British pendulum friction test

A British pendulum tester was used to characterize the friction property of surface textures based on the standard test ASTM E303, which is shown in Fig. 8. Before the test, specimens were fixed on the tester with screws, and the pendulum was locked in a horizontal position. There was a rubber slide at the end of the pendulum. When the pendulum was released, the rubber slider would scrape with the specimen. The scraping distance was made to fall between 124 mm to 127 mm by adjusting the height of the pendulum. Specimens were tested in both dry and wet conditions, and each test was repeated five times to reduce the experimental error.

4. Results and discussions

4.1. Results of the noise absorption test

Results from the noise absorption coefficient tests for group 1, group 2, and group 3 samples are shown in Fig. 9, Fig. 10, and Fig. 11, respectively. Figs. 9–11 indicates that, with the increase in frequency, all the samples exhibit a similar trend of the noise

Fig. 7. Noise-reduction test.

Fig. 8. The British pendulum friction test.

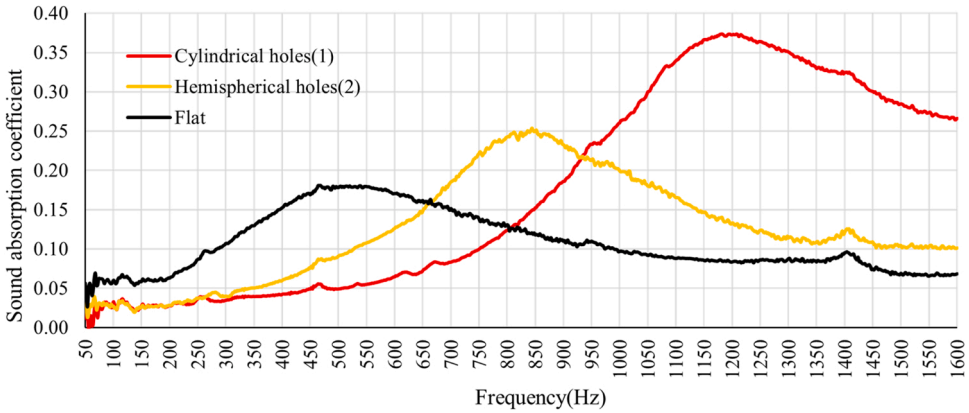

Fig. 9. Results of the noise absorption coefficient test for group 1.

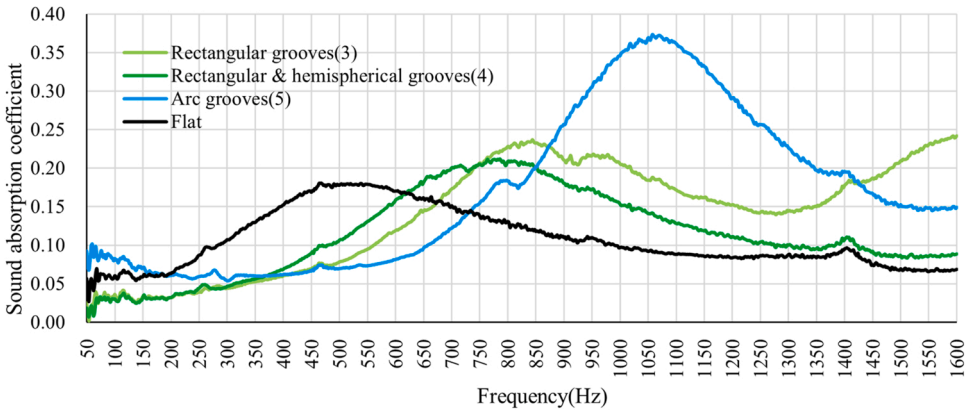

Fig. 10. Results of the noise absorption coefficient test for group 2.

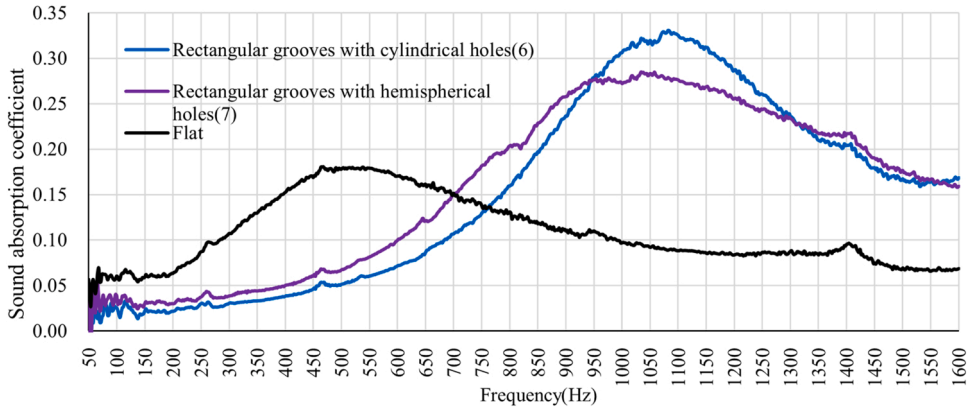

Fig. 11. Results of the noise absorption coefficient test for group 3.

absorption coefficient. The absorption coefficient gradually increases to a peak value and then drops slowly. The peak noise absorption coefficient of the flat sample is 0.17, corresponding to a frequency of 500 Hz. Compared with the flat surface, seven textured surfaces all have higher peak absorption coefficients, corresponding to frequencies ranging from 800 Hz to 1200 Hz. This can be explained by the difference of sound absorption mechanism at low-frequency and high-frequency acoustic waves. Low frequencies, like below 600 Hz, have longer wavelengths. Longer wavelengths mean the sound waves are harder to absorb because they can pass through materials more easily or require thicker materials to effectively dampen them. A flat panel placed in front of the low-frequency sound can act as a resonant absorber. Thus, flat surface will provide better sound impedance at low frequencies. In contrast, textured samples rely on converting sound energy into heat through viscous losses in the material's pores, which commonly work better at higher frequencies. Therefore, textures potentially play a significant role in the noise reduction of concrete pavements, not only in the level of noise abatement but also in the frequencies of mitigated noise.

According to Fig. 9, the type 2 sample has a lower peak noise absorption coefficient than that for type 1, even though the depth of holes for type 1 and type 2 is the same. This may be attributed to the hole shape and difference in the cavity volume created by the two kinds of holes. In group 2 as shown in Fig. 10, type 3 and type 4 show similar results due to the similar texture configurations. The type 5 pattern in group 2, however, has the highest peak absorption coefficient in group 2, which is 0.37 in 1060 Hz. The texture configuration of type 5 is a cavity with a narrow opening and a broadened body (Fig. 2.), which is difficult to construct using traditional texturing techniques. When the noise waves enter the cavity in the type 5 sample, they have to rebound more times to escape from the cavity. More rebounds mean more energy loss. Therefore, noise reduction performance is significantly improved. Fig. 12 illustrates the potential acoustic wave reflection path in textures with traditional rectangular grooves (type 3) and arc grooves (type 5) constructed using this texturing method.

In group 3 as shown in Fig. 11, type 6 performs better than type 7, but the difference between them is smaller than that between type 1 and type 2. The best-performed textures in each group are summarized and shown in Fig. 13, including type 1, type 5, and type 6. As shown in the figure, at the frequency below 1075 Hz, type 5 and type 6 perform better than type 1. At the frequency above 1125 Hz, type 1 performs the best. As aforementioned, the frequency of tire-pavement noise typically ranges from 500 Hz to 1500 Hz. Within this range, type 1 samples (cylindrical holes) demonstrate the highest average absorption coefficient, and type 5 samples perform better than type 6 samples.

4.2. *Results of the skid resistance rest*

The average results of five tests with the error bars for group 1, group 2, and group 3 samples are shown in Fig. 14, Fig. 15, and

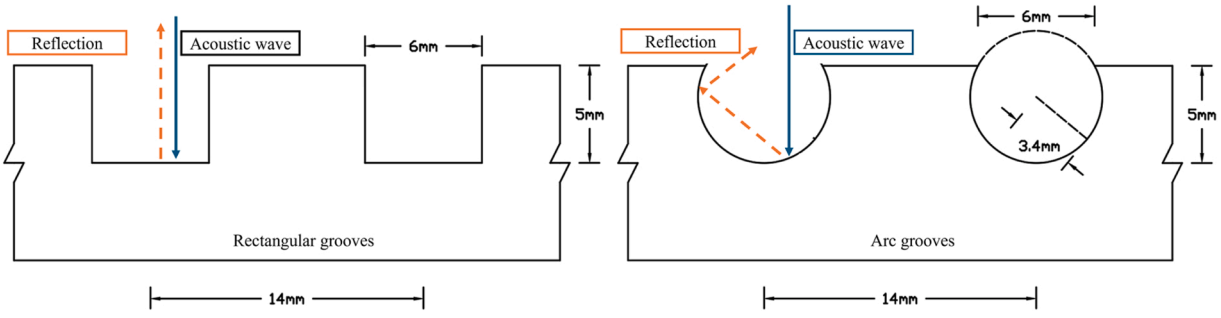

Fig. 12. An illustration of the potential acoustic wave reflection path.

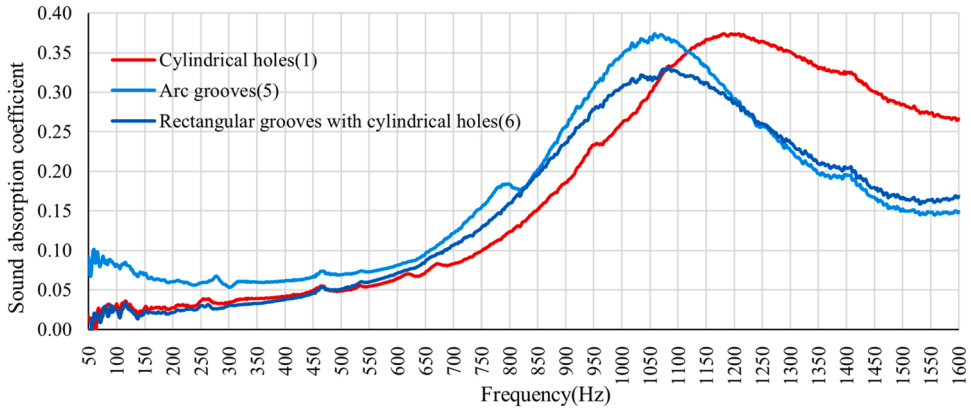

Fig. 13. Comparison of the noise absorption coefficients of type 1, type 5, and type 6 samples.

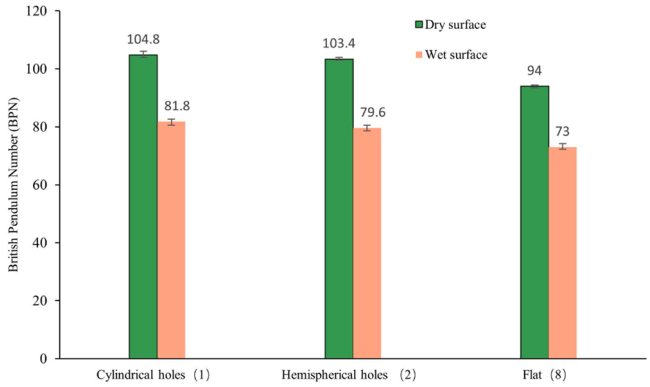

Fig. 14. British pendulum test results for group 1.

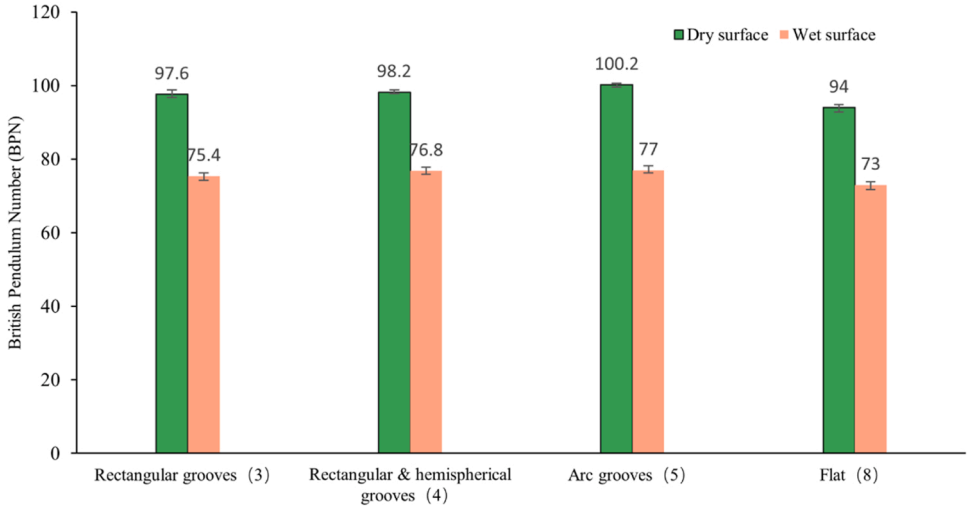

Fig. 15. British pendulum test results for group 2.

Fig. 16, respectively. As shown in the figures, the variations of the test results are very small. As shown in Fig. 14 to Fig. 16, the BPN value of the flat sample is the lowest among all the samples, no matter in a dry or wet condition. The results demonstrate that constructing textures on the pavement surface is an efficient method to improve the skid resistance of concrete pavements. Differences in BPN values between samples among group 1, group 2, and group 3 indicate that the texture configuration is a crucial factor for the anti-

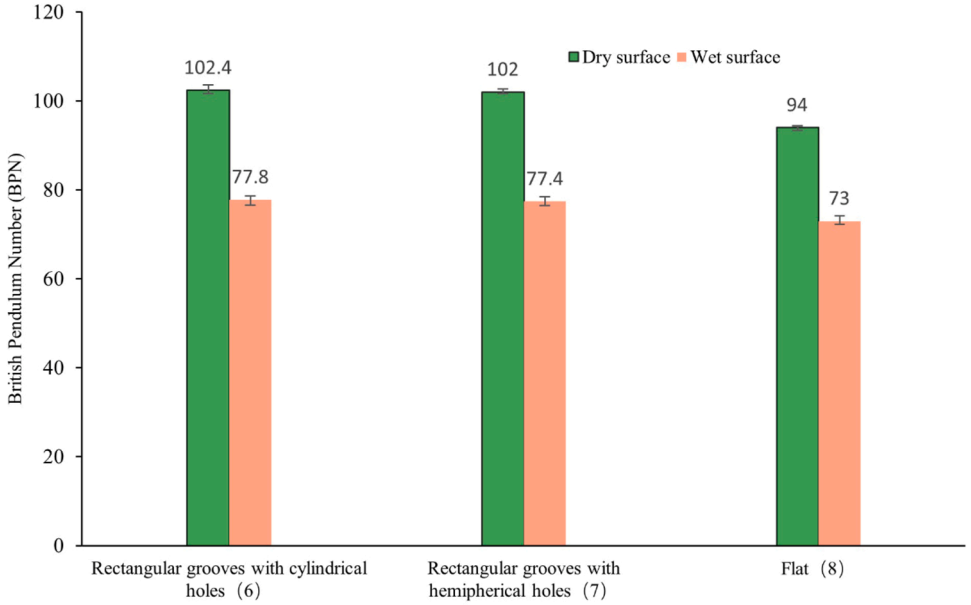

Fig. 16. British pendulum test results for group 3.

skidding performance of pavement textures. In the dry condition, samples with cylindrical or hemispherical holes outperform those with both holes and grooves, which generally outperform those with grooves only. The trends are similar for samples in wet conditions. Samples with cylindrical holes perform the best in both dry and wet conditions.

4.3. Costs and constructability

The costs and constructability of the flexible formworks were evaluated in this study. To apply this fabrication technique to industrial-scale construction of large molds, i.e., size over 1 m x 1 m, laser irradiation techniques such as stereolithography (SLA) is recommended to construct the solid mold because it provides better surface quality than FDM. SLA is the first commercial 3D manufacturing technique developed by Charles Hull in 1986 [43]. Based on the principle of photopolymerization, SLA uses a beam of ultraviolet (UV) laser to irradiate the liquid UV-curable resin from the bottom to the top. When the first layer is solidified, it will drop down with a computer-controlled platform and be covered by fresh liquid resin. The liquid resin is solidified again and adhered to the first layer as the second layer. Once the solid molds are constructed, the manufacturing process of large-scale flexible formworks is similar to that introduced in the laboratory application.

The cost of making large flexible formworks with a size of 1 m× 1 m in size is estimated. The design of a basic solid mold in 1000 mm× 1120 mm× 90 mm is shown in Fig. 17. Two printing schemes of the solid mold are considered, including one-piece printing and four-piece printing. Four-piece printing means printing four pieces with a ¼ size of the whole mold and then assembling these four pieces together. Note that both schemes use SLA technology. Information on production details is shown in Table 2.

As shown in Table 2, printing the mold in one-piece costs nearly double that of fabricating the mold in four pieces because a more expensive SLA machine would be needed for one-piece printing. Thus, four-pieces printing is more favorable in manufacturing solid

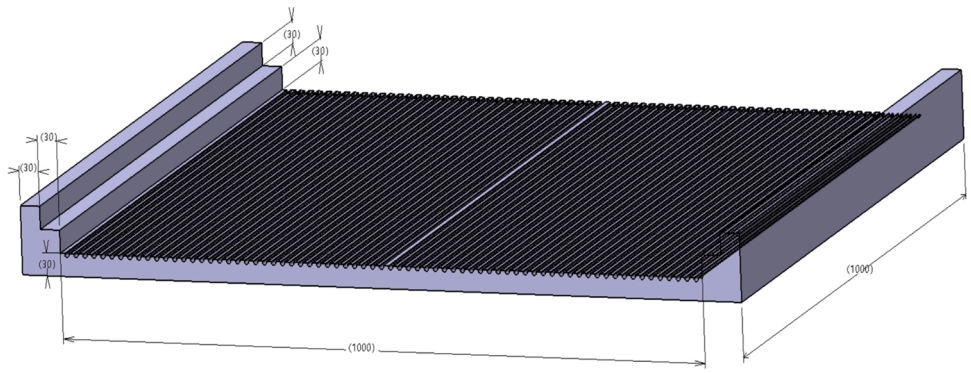

Fig. 17. Configuration of the basic solid mold in large size.

Table 2
3DP based on SLA printing technology.

	One-piece printing	Four-pieces printing
Printing Size (mm)	1000 × 1120 × 90	500 × 560 × 90 (per piece)
Material	Resin	Resin
Technology	SLA	SLA
Thickness	4 mm	4 mm
Cost (US $)	3340	1597 (total for four pieces)

molds. A local supplier offers the price of silicon rubber at 5.8 USD/Kg. It is estimated that 69 Kg of silicon rubber is required to make flexible formworks for a large mold (1 m x 1 m), so the cost of silicon rubber is 400.2 USD. Based on our experience of making flexible formworks with silicone rubber, the flexible formworks can be repeatedly used more than 100 times [44,45]. As a comparison, timber formworks typically do not last more than ten cycles [46]. Assuming that the usage life of the flexible formwork is 100 times, the material cost of flexible formworks to make pavement textures is 4.002 USD/m^2. On the other hand, solid resin mold is hard to damage during the production of flexible formworks. For conservative calculation, the usage life of the solid mold is also assumed to be 100 times. Therefore, the cost of solid molds (Four-pieces printing) to make pavement textures is 0.1597 USD/m^2, and the total material cost to make pavement textures is 4.1617 USD/m^2. No special construction equipment is involved in construction, and added labor cost is very limited. Assume several other related costs to this texturing method: the labor cost is 1.20 USD /m^2 (minimal added labor due to formwork reusability), Equipment Depreciation: 0.30 USD /m^2 (mold fabrication tools amortized over 500 cycles), Energy Consumption: 0.16 USD /m^2 (curing process at 25°C, 48 hours). Then, the total cost is around 5.82 USD/m. NCHRP 634 [47] introduced the cost of traditional texturing method, a direct comparison of cost-effectiveness between this texturing method and other emerging texturing methods are shown in Table 3. Taking into account that the cost in NCHRP 634 was calculated fifteen years ago, it has been adjusted to the 2024 value using an inflation factor of 1.426 based on the Consumer Price Index (CPI) from the Bureau of Labor Statistics (BLS). Based on another report [48], the average cost of diamond grinding ranges from 2 USD/m^2 to 8 USD/m^2, and if there is tough river gravel in concrete, the cost may be up to 12 USD/m^2. While the proposed method is moderately higher in cost than basic techniques (e.g., burlap drag), its customization capability and precision justify the premium compared to high-cost methods like transverse grooving. Moreover, traffic safety improvements and noise reduction bring social benefits that are hard to count in monetary terms.

The constructability of the 3DP flexible formwork is evaluated in a field trial of a heavily loaded road using PCPs. The total length of the trial section is 8 m. The size of the PCP slab is 1 m× 1 m× 0.15 m (thickness), reinforced by fiber-reinforced polymer (FRP) bars. Note that the texture of the slabs is not related to the type of reinforcement used. In producing the slab, the formwork is placed on top of the bottom plate of an assembled slab formwork system (with timber edge formworks). Fresh concrete was placed in the formwork and cured for 28 days, and then the concrete pavement slab was lifted, and the flexible formwork was stripped. For ease of transport and lifting, two steel reinforcement handles are incorporated on both sides of the slab. These handles are specifically designed to provide convenient and secure hoisting points, allowing for safe and efficient handling during transportation and installation processes. The precast concrete road pavement with the pre-designed texture is shown in Fig. 18. Note that the cross-section of textures in the figure is shaped in trapezoid, which is more complicated than those in experiments in order to facilitate better drainage. As shown in the figure, the textures are smooth without noticeable distortions. The field trial results suggest that this new method can be readily used for real construction process.

4.4. Limitations and future research directions

Sample test results indicate that concrete pavement textures play a significant role in the noise absorption and skid resistance of the samples. The noise absorption capacity of different textures is also sensitive to sound frequency. Therefore, it is possible to design and create delicate concrete pavement textures, test their functional performance, and select ones with good performance in both skid resistance and noise abatement. For example, textures made of cylindrical holes are found to perform well in both noise absorption and skid resistance in this study.

However, both pavement noise and skid resistance are complicated issues. Tests at laboratory scale usually do not reflect the true performance of a particular texture in the field. In future studies, full-scale concrete roads can be built with different textures produced with the assistance of 3DP. Alternative test methods such as the On-Board Sound Intensity (OBSI) system and a locked wheel tester can

Table 3
Cost comparison for various surface texturing methods.

Method	Strengths	Cost, USD/m^2
Longitudinal burlap drag	Automated, simple construction	0.17–0.25
Longitudinal tine	High friction, lower noise	0.17–0.25
Transverse groove	Minimal traffic interruption	6.80–13.94
Longitudinal groove	Minimal traffic interruption	2.15–5.10
Longitudinal grind	High friction, low noise	1.69–9.27
The proposed texturing method	Customization of textures	5.82

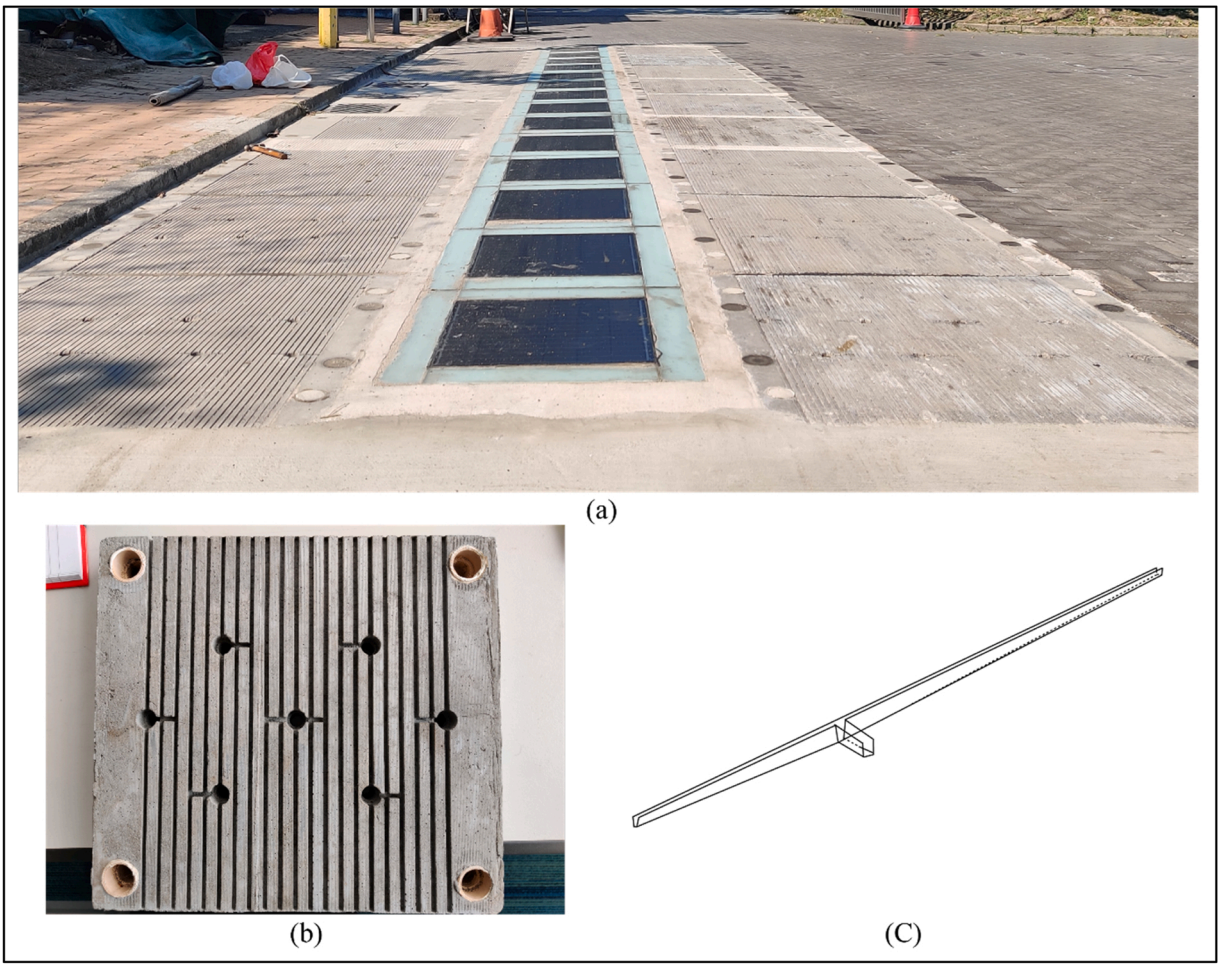

Fig. 18. (a) The field trial of textures created by the flexible formworks; (b) one piece of the precast concrete slab; (c) the schematic diagram of the customized surface texture.

be used to test the tire-pavement noise and skid resistance of the delicate pavement textures, respectively. Nevertheless, 3DP makes it possible to conveniently manufacture a large number of samples with different configurations for field testing.

5. Conclusion and recommendation

Surface texture is critically important in addressing the skid and noise issues of PCPs. However, due to the constraint of available texturing techniques, the configurations of pavement texture are very limited. This study presents a texturing method to construct complex surface textures on PCPs with the assistance of flexible formwork technology and 3DP technology. Solid molds with customized textures were designed using the CAD software and constructed based on the 3DP technology. The pre-textured solid molds were then utilized for the preparation of flexible formworks. Finally, the textured flexible formworks were employed for the cast of PCPs' slabs. Based on this texturing method, laboratory specimens and field trial section of PCPs were implemented for the evaluation of surface performance, constructability and associated costs. This study contributes to the body of knowledge in the research and construction of PCPs' surface textures, and the main conclusions are summarized as follows:

(1) The texturing method developed in this study makes it feasible to create complex and efficient surface textures for PCPs.
(2) Different surface textures designed in this study affect the acoustic performance of the concrete samples. For instance, textures with cylindrical holes absorb more tire-pavement noise.
(3) Different surface textures designed in this study also affect the skid resistance performance of the concrete samples. Textures with cylindrical holes perform the best in skid resistance under both dry and wet conditions.
(4) The associated costs of using this texturing method to construct PCPs' surface textures are competitive with those of traditional texturing techniques.
(5) The designed textures in the trial section of PCPs are smooth and uniform, and no obvious defects were found after construction.

Although this study shows the promising potentials of designing high-performance surface textures for precast concrete pavements assisted with 3DP technology, it is recommended that more research be conducted in the future to more thoroughly test and monitor the texture performance and improve the texture patterns. Several specific recommendations on future research are given as follows:

(1) The influence of mix design for concrete materials on the formation and precision of created textures should be further investigated.
(2) More performance-related properties, such as the surface drainage and the durability of textures, should be considered with skid resistance and noise reduction performance to comprehensively develop superior pavement textures.
(3) Pavement surface mechanics should be thoroughly investigated to reasonably design the configurations of textures.
(4) On actual road pavements, tire-pavement noise is not only affected by absorption coefficient but also by noise generation mechanisms between tire and pavement. Skid resistance is also largely affected by the contact area and penetration of the tire into the pavement surface. Therefore, more relevant tests can be performed on full-scale road pavements.
(5) A more comprehensive lifecycle cost analysis is needed for this proposed texturing method incorporating long-term maintenance and durability of created textures.

CRediT authorship contribution statement

CHEN Xingyu: Writing – original draft, Methodology, Formal analysis, Data curation, Conceptualization. **Wang Yuhong:** Writing – review & editing, Supervision, Methodology, Funding acquisition, Conceptualization. **Sheng Wei:** Writing – review & editing, Investigation, Data curation. **Zhu Xingyi:** Writing – review & editing, Resources, Funding acquisition. **Chan Longyee:** Investigation, Data curation.

Declaration of Competing Interest

The authors declare that they have no known competing financial interests or personal relationships that could have appeared to influence the work reported in this paper.

Acknowledgment

The research work presented in this paper was supported by the National Key R&D Program of China (No.2023YFE0202400), the Innovation and Technology Commission (ITC) of Hong Kong (Project no. MHP/150/22) and the Research Grants Council (Project no. R5007–18).

Data availability

Data will be made available on request.

References

[1] A. Syed, R.S. Sonparote, Development and early-age performance of an innovative prestressed precast concrete pavement, J. Constr. Eng. Manag. 146 (2) (2020) 05019018.
[2] M. Fang, R. Zhou, W. Ke, B. Tian, Y. Zhang, J. Liu, Precast system and assembly connection of cement concrete slabs for road pavement: a review, J. Traffic Transp. Eng. (Engl. Ed. 9 (2) (2022) 208–222.
[3] S. Tayabji, S. Tyson, Precast concrete pavement implementation, Concr. Int. 39 (4) (2017).
[4] Y. Sugiyama, R.J. Stump, A. Nguyen, L. Wen, Y. Chen, Y. Wang, J.N. Murdoch, F.J. Lovicu, J.W. McAvoy, Secreted frizzled-related protein disrupts PCP in eye lens fiber cells that have polarised primary cilia, Dev. Biol. 338 (2) (2010) 193–201.
[5] B. Qu, X.Z. Weng, J. Zhang, J.J. Mei, T.X. Guo, R.F. Li, S.H. An, Analysis on the deflection and load transfer capacity of a prefabricated airport prestressed concrete pavement, Constr. Build. Mater. 157 (2017) 449–458.
[6] L. Yu, X. Yang, X. Yan, X. Zhang, T. Zhao, C. Duan, J. Mills-Beale, Design and construction of oblique prestressed concrete pavement: a case study in China, Appl. Sci. 8 (4) (2018) 607.
[7] J. Zhang, X. Weng, B. Yang, Y. Li, J. Liu, L. Jiang, Bonding characteristics of grouting layer in prefabricated cement concrete pavement, Constr. Build. Mater. 145 (2017) 528–537.
[8] J. Novak, A. Kohoutková, V. Křístek, J. Vodička, Precast concrete pavement–systems and performance review, in: In IOP Conference Series: Materials Science and Engineering, 236, IOP Publishing, 2017, September 012030.
[9] S. Tayabji, D. Ye, N. Buch, SHRP 2 Report S2-R05-RR-1: Precast concrete pavement technology, Transportation Research Board of the National Academies, Washington, DC, 2013.
[10] FHWA (Federal Highway Administration). (2016). "How Do Weather Events Impact Roads?" Webpage. <⟨https://ops.fhwa.dot.gov/weather/q1_roadimpact.htm⟩> .Federal Highway Administration, Washington, DC.
[11] U. Sandberg, J.A. Ejsmont, Tyre/Road Noise Reference Book, ISBN 91-631-2610-9, Informex, Handelsbolag, Kisa, Sweden, 2002.
[12] Todd E. Honerner, Smith, D. Kurt, Larson, M. Roger, Mark E. Swanlund, Current practice of portland cement concrete pavement texturing, Transp. Res. Rec. 1860 (1) (2003) 178–186.
[13] ACPA (American Concrete Pavement Association), Concrete Pavement Surface Textures, Special Report. Report No. SR902P, American Concrete Pavement Association, Skokie, IL, 2000.
[14] NCPTC National Concrete Pavement Technology Center, "Texturing concrete pavement for reduced tire/pavement noise using longitudinal tining, Guide Specif. Highw. Constr. (2011) 3–11 (CPSCP GS).
[15] G. Lu, Y. He, Z. Leng, D. Wang, B. Hong, J. Xiong, J. Wei, M. Oeser, Comparison of the polishing resistances of concrete pavement surface textures prepared with different technologies using the Aachen polishing machine, J. Mater. Civ. Eng. 33 (9) (2021) 04021226.

[16] J. Yu, B. Zhang, P. Long, B. Chen, F. Guo, Optimizing the texturing parameters of concrete pavement by balancing skid-resistance performance and driving stability, Materials 14 (20) (2021) 6137.
[17] Z. Cai, J. Fan, T. Ma, X. Deng, Y. Zhu, Aggregate-exposing operation parameters, laboratory and road performances of exposed-aggregate concrete pavement applied in long tunnel, J. Test. Eval. 51 (2) (2023) 416–434.
[18] Z. Leng, Z. Fan, P. Liu, J. Kollmann, M. Oeser, D. Wang, X. Jiang, Texturing and evaluation of concrete pavement surface: a state-of-the-art review, J. Road. Eng. (2023).
[19] Jens Skarabis, Ulrike Stöckert, Noise emission of concrete pavement surfaces produced by diamond grinding, J. Traffic Transp. Eng. (Engl. Ed.) 2 (2) (2015). Page81-92.
[20] L. Chu, J. Peng, Y. Liu, T.F. Fwa, Effectiveness of pavement grooving in skidding prevention on horizontal curves, J. Transp. Eng., Part B: Pavements 148 (4) (2022) 04022054.
[21] Z. Cong, H. Chen, N.X. Zheng, W. Zhou, Surface texture of cement concrete pavement: a review, Mater. Rep. 34 (9) (2020) 9110–9116.
[22] P.R. Donavan, Noise evaluation of various pavement textures on new Portland cement concrete, Noise Control Eng. J. 57 (2) (2009) 63–76.
[23] I.M. Guada, A. Rezaei, J.T. Harvey, D. Spinner, 2012, Evaluation of grind and groove (next generation concrete surface) pilot projects in California.
[24] Cauberg, N., Parmentier, B., Vanneste, M. and Mollaert, M., 2009. Fabric formwork for flexible, architectural concrete. In Proceedings of the international symposium on fibre-reinforced polymer reinforcement for concrete structures, FRPRCS-9. Sydney, Australia.
[25] B. Kromoser, J. Kollegger, Pneumatic forming of hardened concrete–building shells in the 21st century, Struct. Concr. 16 (2) (2015) 161–171.
[26] D. Veenendaal, P. Block, Design process for prototype concrete shells using a hybrid cable-net and fabric formwork, Eng. Struct. 75 (2014) 39–50.
[27] W.J. Hawkins, M. Herrmann, T.J. Ibell, B. Kromoser, A. Michaelski, J.J. Orr, R. Pedreschi, A. Pronk, H.R. Schipper, P. Shepherd, D. Veenendaal, Flexible formwork technologies–a state of the art review, Struct. Concr. 17 (6) (2016) 911–935.
[28] Tuan D. Ngo, Alireza Kashani, Gabriele Imbalzano, Kate T.Q. Nguyen, David Hui, "Additive manufacturing (3D printing): a review of materials, methods, applications and challenges, Compos. Part B: Eng. 143 (2018) 172–196.
[29] D.D. Camacho, P. Clayton, W.J. O'Brien, C. Seepersad, M. Juenger, R. Ferron, S. Salamone, Applications of additive manufacturing in the construction industry–a forward-looking review, Autom. Construct. 89 (2018) 110–119.
[30] C.K. Chua, K.F. Leong, C.S. Lim, Rapid Prototyping: Principles and Applications (with Companion CD-ROM) Third Edition, World Scientific Publishing Company, 2010.
[31] H.Q. Sun, J.J. Zeng, G.Y. Hong, Y. Zhuge, Y. Liu, Y. Zhang, 3D-printed functionally graded concrete plates: concept and bending behavior, Eng. Struct. 327 (2025) 119551.
[32] J. Xiao, G. Ji, Y. Zhang, G. Ma, V. Mechtcherine, J. Pan, L. Wang, T. Ding, Z. Duan, S. Du, Large-scale 3D printing concrete technology: Current status and future opportunities, Cem. Concr. Compos. 122 (2021) 104115.
[33] J.J. Zeng, X. Hu, H.Q. Sun, Y. Liu, W.J. Chen, Y. Zhuge, Triaxial compressive behavior of 3D printed PE fiber-reinforced ultra-high performance concrete, Cem. Concr. Compos. 155 (2025) 105816.
[34] Behrokh Khoshnevis, Automated construction by contour crafting—related robotics and information technologies, Autom. Constr. 13 (1) (2004) 5–19.
[35] S.C. Paul, G.P. Van Zijl, M.J. Tan, I. Gibson, A review of 3D concrete printing systems and materials properties: current status and future research prospects, Rapid Prototyp. J. 24 (4) (2018) 784–798.
[36] R. Truby, J. Lewis, Printing soft matter in three dimensions, Nature 540 (2016) 371–378, https://doi.org/10.1038/nature21003.
[37] J. Guo, T.M. Chan, Experimental and numerical study on the structural performance of the stainless steel ring strengthened removable dowel bar connection system, Int. J. Pavement Eng. 24 (2) (2023) 2126977.
[38] Z. Wang, Y. Huang, X. Zhang, L. Li, M. Chen, D. Fang, Broadband underwater sound absorbing structure with gradient cavity shaped polyurethane composite array supported by carbon fiber honeycomb, J. Sound Vib. 479 (2020) 115375.
[39] X.D. Fan, Y.F. Zhu, B. Liang, J. Yang, J. Yang, J.C. Cheng, Ultra-broadband and planar sound diffuser with high uniformity of reflected intensity, Appl. Phys. Lett. 111 (10) (2017).
[40] Omar A. Mohamed, Masood, H. Syed, Jahar L. Bhowmik, Optimization of fused deposition modeling process parameters: a review of current research and future prospects, Adv. Manuf. 3 (1) (2015) 42–53.
[41] C.J., Luis Perez, Analysis of the surface roughness and dimensional accuracy capability of fused deposition modeling processes, Int. J. Prod. Res. 40 (12) (2002) 2865–2881.
[42] X. Chen, Y. Wang, H. Chong, J. Huang, Use of sulphoaluminate cement in grouted macadam as sustainable pavement material, J. Transp. Eng., Part B: Pavements 146 (2) (2020) 04020018.
[43] Ferry P.W. Melchels, Jan Feijen, Dirk W. Grijpma, A review on stereolithography and its applications in biomedical engineering, Biomaterials 31 (24) (2010) 6121–6130.
[44] W. Sheng, Y. Wang, Fatigue behavior and abrasion resistance of prefabricated pavement textures assisted with 3D printing technology. In Green and Intelligent Technologies for Sustainable and Smart Asphalt Pavements, CRC Press, 2021, pp. 266–271.
[45] W. Sheng, Y. Wang, Traffic noise mitigation through texture-induced quiet pavement: analytical modeling and field test, Transp. Res. Part D: Transp. Environ. 137 (2024) 104485.
[46] Yip, R. and Poon, C.S., 2008, February. Comparison of timber and metal formwork systems. In Proceedings of the Institution of Civil Engineers-Waste and Resource Management (Vol. 161, No. 1, pp. 29-36). Thomas Telford Ltd.
[47] National Academies of Sciences, Engineering, and Medicine, 2009. Texturing of Concrete Pavements.
[48] ACPA (American Concrete Pavement Association). (2001). "Diamond Grinding and Concrete Pavement Restoration." Technical Bulletin TB-008P.